Electronic band structure, magnetic, transport and thermodynamic properties of In-filled skutterudites InxCo4Sb12

Juliusz Leszczynski, Véronique Da Ros, Bertrand Lenoir, Anne Dauscher, Christophe Candolfi, Philippe Masschelein, Jiri Hejtmanek, Kamil Kutorasinski, Janusz Tobola, Ron I. Smith, et al.

Electronic band structure, magnetic, transport and thermodynamic properties of In-filled skutterudites $In_xCo_4Sb_{12}$

J Leszczynski[1], V Da Ros[1], B Lenoir[1], A Dauscher[1], C Candolfi[1], P Masschelein[1], J Hejtmanek[2], K Kutorasinski[3], J Tobola[3], R I Smith[4], C Stiewe[5] and E Müller[5]

[1]CNRS-Université de Lorraine (UMR 7198), Institut Jean Lamour, Parc de Saurupt, CS 50840, F-54011 Nancy, France

[2]Institut of Physics, Academy of Sciences of the Czech Republic, Cukrovarnicka 10, CZ-162 53 Praha 6, Czech Republic

[3]Faculty of Physics and Applied Computer Science, AGH University of Science and Technology, 30-059 Krakow, Poland

[4]ISIS Facility, Rutherford Appleton Laboratory, Harwell Oxford, Didcot, OX11 0QX, United Kingdom

[5]German Aerospace Center (DLR), Institute of Materials Research, Linder Hoehe, 51147 Cologne, Germany

Corresponding author: bertrand.lenoir@univ-lorraine.fr

Abstract

The thermoelectric and thermodynamic properties of polycrystalline $In_xCo_4Sb_{12}$ ($0.0 \leq x \leq 0.26$) skutterudites were investigated and analyzed between 2 and 800 K by means of electrical resistivity, thermopower, thermal conductivity and specific heat measurements. Hall effect, sound velocity and thermal expansion measurements were also made in order to gain insights into the transport and elastic properties of these compounds. The impact of the In filling on the crystal structure as well as the thermal dynamics of the In atoms were tracked down to 4 K using powder neutron diffraction experiments. Analyses of the transport data were compared with the evolution of the electronic band structure with x determined theoretically within the Korringa-Kohn-Rostoker method with the coherent

potential approximation (KKR-CPA). These calculations indicate that In gives rise to a remarkable large *p*-like density of states located at the conduction band edge. The electrical properties show typical trends of heavily-doped semiconductors regardless of the In content. The thermal transport in $CoSb_3$ is strongly influenced by the presence of In in the voids of the crystal structure resulting in a drop in the lattice thermal conductivity values in the whole temperature range. The low value of the Grüneisen parameter suggests that this decrease mainly originates from enhanced mass-fluctuations and point-defect scattering mechanisms. The highest thermoelectric figure of merit $ZT \sim 1.0$ at 750 K was achieved at the maximum In filling fraction *i.e.* for $x = 0.26$.

PACS: 74.25.Fy, 72.15.Jf, 31.15.A-, 75.30.Cr

1. Introduction

Skutterudites based on $CoSb_3$ are currently extensively studied for their prospective thermoelectric properties typified by high values of the dimensionless figure of merit ZT defined as $ZT = \alpha^2 T / \rho(\kappa_e + \kappa_L)$ [1-3]. In this formula, T is the absolute temperature, α is the thermopower or Seebeck coefficient, ρ is the electrical resistivity, κ_e and κ_L the electronic and lattice thermal conductivities, respectively. High ZT values thus arise from a beneficial combination of high power factor α^2 / ρ and low thermal conductivity $(\kappa_e + \kappa_L)$. While the former is primarily dictated by the carrier concentration, the latter is achieved by inserting foreign species into the voids of the crystal structure of $CoSb_3$ [2-3]. Filling these empty sites results in partially-filled skutterudites of general formula $M_xCo_4Sb_{12}$ where *M* can be chosen among a large variety of elements ranging from alkali to rare-earth atoms [4-14]. Their presence leads to the concomitant enhancement of mass contrast between empty and filled voids and the development of localized modes, both of which efficiently disrupt the acoustic heat-carrying phonons. The influence of this last mechanism, referred in literature as “rattling”, on κ_L may be explained either in terms of resonant scattering *i.e.* decoupled guest vibrations with respect to the host framework or in terms of a local reduction in the phonon group velocity around the frequency of the guest vibrational mode. Independently of the exact underlying mechanism at play, the

drastic influence of the guest atoms on κ_L was widely confirmed experimentally for numerous filler elements[4-14]. This approach was recently extended to double- and even triple-filled skutterudites for which several guest atoms are inserted in order to affect the phonon spectrum in a wider frequency range, thereby further reducing κ_L [3,15-22]. Such optimization proved to be fruitful in maximizing the ZT value which was significantly raised from a mean value of 1.0 at 800 K in single-filled compounds to 1.7 at 850 K in the triple-filled $Ba_{0.08}La_{0.05}Yb_{0.04}Co_4Sb_{12}$ skutterudite [22].

This strategy, however, relies on a detailed understanding of the influence of a given filler atom *M* on both the electronic and thermal properties. The former is intimately related to the effective number of electrons per atom *M* transferred to the host framework, which, when estimated, enables a fine tuning of the carrier concentration and hence, the power factor. The latter is straightforwardly captured through the thermal atomic displacement parameter (ADP), which relates the temperature dependence of the ADP values of the *M* atoms to their Einstein temperature. This last parameter, also encoded in the low-temperature specific heat data, is particularly useful to select a suitable combination of elements to further decrease κ_L within a multiple-filling approach. Though these issues were partially or fully addressed for several atoms such as Tl, Ba, Ce or Ca, a complete understanding is still lacking for In [5,7,11,12].

While a richer literature on double-filled skutterudites with In exists [19-21,23-25], only few studies focused on In-partially-filled $CoSb_3$ to date. Following the first investigation of He *et al*. [4] that determined the solubility limit of In and determined the high-temperature thermoelectric properties, Peng *et al*. [26] recently reported specific heat and inelastic neutron scattering data on the compositions $In_{0.2}Co_4Sb_{12}$ and $In_{0.2}Yb_{0.2}Co_4Sb_{12}$. This study revealed the presence of a low-energy phonon mode centred at 5 meV consistent with an Einstein temperature of the In atoms of ~ 60 K. Another strategy to improve the thermoelectric performance of skutterudites using In benefitted from the metastable nature of this filler element to synthesize bulk nanocomposite compounds [23,27]. When an excess of both In and Sb is introduced, finely dispersed nanoparticles of InSb appear. Not only do these embedded nanoparticles enhance phonon scattering at the interface between the InSb and skutterudite phases, but they also induce higher thermopower values presumably due to distortion of the density of states near

the Fermi level. Finally, Mallik et al. studied the influence of off-stoichiometry by In addition on the high-temperature thermoelectric properties and found a maximum ZT of up to 1.12 at 650 K. [28,29]

Note that this approach is not restricted to In and was extended to Ga *i.e.* another group IIIA element [18]. This last species was recently shown to behave as an amphoteric dopant in $CoSb_3$ due to its propensity to be located either into the voids or on the Sb site [30]. Such dual-site occupancy coincides with transport properties measurements suggesting that these compounds can be classified as charge-compensated semiconductors. The possibility to insert Ga in the empty cages or to realize a partial compensation offers a new degree of freedom to optimize the thermoelectric properties of $CoSb_3$-based skutterudites and further raises the question whether In shares similar behavior.

Here, we provide a detailed study of the transport and thermodynamic properties in a broad temperature range (2 – 800 K) of In-filled skutterudites $In_xCo_4Sb_{12}$ for $0.0 \leq x \leq 0.26$ with the aim of obtaining a full description of the impact of In on the transport properties of $CoSb_3$. The experimental findings are complemented by and compared with electronic band structure calculations performed to determine the evolution of the dispersion curves and density of states with x. The paper is organized as follows. After presenting the results of the structural and chemical characterizations (Section 3.1), we describe the electronic band structure focusing on the similarities and differences between these compounds and other partially-filled skutterudites (Section 3.2), in particular with Ca and Ba. The subsequent sections are dedicated to the magnetic susceptibility data (Section 3.3) followed by the presentation and discussion of the electrical properties results, which include electrical resistivity, thermopower and Hall effect (Section 3.4). The thermal transport data combining specific heat and thermal conductivity are discussed in Section 3.5. Finally, the high-temperature thermoelectric data are presented in the last section (Section 3.6).

2. Experimental and computational details

2.1. Synthesis, crystal structure and chemical homogeneity

Polycrystalline $In_xCo_4Sb_{12}$ samples with nominal compositions x = 0.0, 0.10, 0.20, 0.30 and 0.40 were synthesized by loading stoichiometric amounts of high purity In shots (99.999%), Sb shots (99.999%) and Ni-free Co powders (99.998%) into an evacuated quartz ampoule. The use of Ni-free Co

powders is justified by the fact that even a minute amount of Ni impurities may have a significant impact on the transport properties as recently demonstrated in the $Ca_xCo_4Sb_{12}$ skutterudites [31]. The ampoules were sealed under a reducing He-H_2 (95-5%) atmosphere and heated in a vertical oscillating furnace up to 1023 K. The quartz tubes were maintained at this temperature for 96h and then quenched in cold water. The obtained ingots were ground in an agate mortar into powders and sieved to get micron-sized particles (~ 100μm). The powders were cold-pressed into pellets and annealed under the same previous atmosphere conditions at 893 K for 96h. After a final grinding step (< 50μm), the final densification was achieved by hot pressing under inert atmosphere in graphite dies at 923 K for 2h and under an applied pressure of 50 MPa. The relative density of the samples, defined as the ratio of the experimental density to the theoretical density, was found to be above 92% regardless of the In content. The former was determined from the geometrical dimensions and the weight of the samples while the latter was obtained from crystallographic data.

Crystal structure investigation was carried out by x-ray powder diffraction (XRPD) at room temperature. To shed light on the thermal motion of the In atoms, neutron powder diffraction (NPD) patterns at low and ambient temperatures (4 – 300 K) were collected on the diffractometer POLARIS (ISIS, UK) with the samples contained in thin-walled vanadium cylinders. Crystal structure refinement from the NPD patterns was done by the Rietveld method using the Fullprof software [32].

The chemical homogeneity of the samples was checked by electron probe microanalysis (EPMA). The actual compositions were determined by averaging over 25 to 30 distinct spots on the surface of each sample and by normalizing the resulting chemical formulae to four cobalt atoms.

2.2 Transport, magnetic, thermodynamic and elastic properties measurements

Transport property measurements were conducted on bar-shaped samples (typically 2×2×8 mm^3) cut from the densified ingots with a diamond wire-saw. Electrical resistivity, thermopower and thermal conductivity were simultaneously measured between 2 and 350 K using the thermal transport option (TTO) of a physical property measurement system (PPMS, Quantum Design) by soldering four copper bars onto the samples with a BiSn braze. Hall effect measurements were performed by a five-contact method. Ohmic contacts were made by connecting five thick Cu wires onto the samples using BiSn. The

transverse electrical resistivity was then measured with an ac transport option of the PPMS over the 2 – 300 K temperature range by sweeping the magnetic field from -7 to +7 T. Specific heat (C_p) measurements on small pieces (~ 10 mg) were performed in the temperature range 2 – 300 K with the dedicated option of the PPMS using the thermal relaxation method.

Magnetic susceptibility χ was measured using a Quantum Design superconducting quantum interference device (SQUID) magnetometer under magnetic fields $\mu_0 H$ of up to 5T between 5 and 300 K.

Sound velocity measurements were carried out at room temperature on cylindrical-shaped samples (Ø ~ 15mm and ~ 4mm thickness) to determine the transverse and longitudinal velocities of sound using a conventional ultrasonic pulse-echo method.

Thermopower and electrical resistivity were simultaneously measured between 300 and 800 K on the same samples used for TTO measurements by a standard steady-state method using a home-made apparatus. Thermal conductivity was determined in the same temperature range by measuring the thermal diffusivity D via a laser flash technique on disk-shaped samples. Both quantities are related by the formula $\kappa = DC_p\rho_V$ where ρ_V is the experimental density of the sample. C_p and ρ_V measurements were conducted on a Netzsch DSC (Differential Scanning Calorimetry) and dilatometer, respectively, between 300 and 800 K.

2.3 First-principles calculations

Electronic band structure calculations were performed using the Korringa-Kohn-Rostoker method combined with the coherent potential approximation (KKR-CPA) to treat the chemical disorder on the vacancy/In crystallographic site [33,34]. The self-consistent crystal potentials of the muffin-tin form were constructed within the local density approximation (LDA) utilizing the von Barth-Hedin formula for the exchange-correlation part. Energy dispersion curves were calculated along high-symmetry directions in the Brillouin zone. For fully-converged crystal potentials and atomic charges, total-, site- and orbital-decomposed density of states (DOS) were generated using a tetrahedron method for integration in the reciprocal *k*-space. Precise determination of the Fermi level was made by using the

generalized Lloyd formula. The experimental relevant crystallographic parameters derived from both XRPD and NPD experiments were used in these calculations.

3. Results and discussion

3.1 Crystal structure and chemical characterizations

Both XRPD and NPD patterns show that all the samples possess a cubic structure that can be indexed in the space group $Im\bar{3}$ (Figure 1). EPMA results further confirmed the presence of small fractions of InSb and revealed a good chemical homogeneity of the skutterudite phase. The relevant crystallographic parameters derived from NPD along with the actual compositions measured by EPMA are listed in Table 1. Further attempts to increase the In content by starting from higher nominal x values led to increasing amounts of secondary phases without significant variations in the lattice parameter. These results thus suggest that the solubility limit of In in the $CoSb_3$ compound is ~ 0.26 *i.e.* close but slightly higher than the value of 0.22 determined by He *et al*. [4] and by Mallik *et al*. [28,29]. Hereafter, the actual values of x will be used to label the samples.

The lattice parameter a, determined from Rietveld refinements against the XRPD data, increases linearly with the In content following Vegard's law to within experimental accuracy. The maximum value of a measured for the x = 0.26 sample is slightly lower than that obtained by He *et al*. [4] (9.052 Å here with respect to 9.056 Å). As shown by Puyet et al. [31], the purity of the Co powders used as starting element plays a crucial role in both the crystal structure and transport properties. Minute amount of Ni impurities (~ 400 ppm) increases the lattice parameter from 9.043 Å (Ni-free) to 9.048 Å (Ni-containing). The discrepancy between our result and that of He et al. might thus originate from this effect. In addition, a similar effect, with Fe impurities for instance (Fe leads to a decrease in a), may also explain the lower lattice parameter found by Mallik et al. [28] (9.0425 Å for x = 0.25) who used elemental Co of lower purity (99.95%). Taken as a whole, our results seem consistent with a higher solubility limit of In in the skutterudite phase. For NPD refinements, shown in Figure 1 for the illustrative x = 0.26 sample, the Co and Sb sites were fixed to full occupancy regardless of the In content and temperature. Refinements of the In site occupancy produced compositions corresponding to the

compositions measured by EPMA within the uncertainty which arises from correlations between site occupancy and atomic displacement parameters. Subsequently, the In fractions were kept constant to the EPMA values. The anisotropic thermal displacement parameters of In, Co and Sb were determined in a final stage of the refinement. Note that neither deficiency on the Co and Sb sites nor possible substitution of In for Sb were evident from refinements. We therefore conclude that no vacancies are present in the Co-Sb matrix and that In is solely located into the voids of the skutterudite structure in the present series of samples. Yet, based on these results, the possibility to substitute In for Sb cannot be excluded and clearly deserves further work.

Figure 2 shows the temperature dependence of a for the x = 0.26 sample obtained from NPD refinements (see Table 2 for relevant crystallographic parameters of the x = 0.26 sample as a function of temperature). The slope of the linear decrease of a with temperature is related to the linear thermal expansion coefficient α_T defined as

$$\alpha_T = \left(\frac{1}{a} \frac{\partial a}{\partial T} \right)_P \tag{1}$$

The $a(T)$ data collected between 150 and 300 K yields α_T = 9.10^{-6} K^{-1}, in line with thermal expansion coefficients reported in other partially-filled skutterudites [35]. This result is also in reasonable agreement with the value directly obtained from dilatometric measurement performed at higher temperatures (300 – 800 K) giving α_T ~ 6.7×10^{-6} K^{-1}.

The characteristic Einstein temperature θ_E describing the thermal motion of the In atoms can be inferred from the temperature dependence of their isotropic ADP values U_{iso} via the relation

$$U_{iso} = \frac{h^2}{8\pi^2 m k_B \theta_E} \coth \frac{\theta_E}{2T} + d^2 \tag{2}$$

where h is the Planck constant, m is the mass of the atom expressed in atomic mass unit, k_B is the

Boltzmann constant and d^2 is a parameter describing the temperature-independent disorder. Fitting the $U_{iso}(T)$ curve to Eq.(2) gives θ_E ~ 67 K and d^2 ~ 0.002 Å^2. The value of θ_E is in good agreement with that found by Peng *et al*. [26] from $C_p(T)$ and inelastic neutron scattering data collected on a sample with similar In content. The value of the parameter d^2 is consistent with those observed for other filler elements and is close to zero indicating little static disorder [36].

The isotropic ADP values of the host framework atoms can be utilized to estimate the Debye temperature θ_D of the skutterudite framework

$$U_{iso} = \frac{3h^2T}{4\pi^2 m k_B \theta_D^2}\left(\frac{T}{\theta_D}\int_0^{\theta_D/T}\frac{x}{e^x-1}dx + \frac{\theta_D}{4T}\right) + d^2 \qquad (3)$$

An averaged ADP and mass m of the Co-Sb framework was calculated according to site occupancy values. This model leads to d^2 ~ 0.02 Å^2 and θ_D ~ 295 K. The value of θ_D is very close to that derived for the parent compound $CoSb_3$ as commonly observed in partially-filled skutterudites [35].

Independently from these crystallographic characteristics, θ_D can be inferred from ultrasound velocity measurement. In this approach, the longitudinal and transverse velocities v_L and v_T, respectively, are used to define an average velocity of sound v_m following the Anderson's relation [37]

$$\frac{3}{v_m^3} = \frac{2}{v_T^3} + \frac{1}{v_L^3} \qquad (4)$$

Here, the experimental values of v_L and v_T, 4715 $m.s^{-1}$ and 2788 $m.s^{-1}$, respectively, result in v_m = 3089 $m.s^{-1}$. Within the Debye model, the relation between v_m and θ_D is then given by

$$\theta_D = \frac{h}{k_B}\left(\frac{3nN_A d}{4\pi M}\right)^{1/3} v_m \qquad (5)$$

where n is the number of atoms per unit cell, N_A is the Avogadro's number and M is the molar mass. Eq.(5) gives θ_D ~ 320 K in good agreement with that derived from $U_{iso}(T)$ data. The slight discrepancy between these two values is likely due to the limited experimental accuracy (mainly due to the strong absorption of In) in the estimation of the isotropic displacement parameters.

3.2 Electronic band structure calculations

Figure 3 shows the energy dependence of the total density of states (DOS) for three In concentrations in $In_xCo_4Sb_{12}$ while the site-decomposed DOS for x = 0.04 and 0.26 are depicted in Figure 4. These results indicate that the main contribution near E_F comes from the Co *d*-states and Sb *p*-states. Regardless of the filling fraction x, the In contribution to $N(E_F)$ solely originates from *p*-states. Interestingly, these states lead to a sharp DOS peak that nears the Fermi level for x = 0.04. The situation is reminiscent to Ca partially-filled skutterudites for which the *s*-states of Ca are confined in a narrow peak near the conduction band edge (see Figure 5) [7]. Further, these *s*-states were found to shift towards higher energy upon increasing the total number of electrons on going from Ca to Ba (in spite of the same number of valence electrons) [7]. This shift gives rise to dominant states of *d* symmetry near the conduction band edge in the case of Ba, likely due to more attracting crystal potential with respect to those of Ca. Here, the situation appears as intermediate since replacing Ca by In and then by Ba changes the dominant states near E_F from *s* to *p* and eventually to *d* symmetry, respectively. Likewise the Ca case, this sharp DOS peak broadens as the In content increases due to stronger hybridization with the Co *d*-states and Sb *p*-states. Concomitantly, the Fermi level is slightly shifted deeper inside the conduction bands indicating highly-doped semiconducting behavior.

In order to examine a possible amphoteric behavior of In akin to that of Ga [30], KKR-CPA calculations were performed on the, so far, hypothetical compound $Co_4Sb_{12-y}In_y$ for y = 0.04. Unlike the above-mentioned case, the Fermi level moves inside the valence bands (Figure 6) indicating a *p*-type character of these compounds. The *p*-symmetry states of In are located below the band gap since In possesses two electrons less than Sb. Hence, In behaves as a double hole donor leading to positive thermopower values. The possible position of In into the voids and on the Sb site would then give rise to

compensation effects resulting in an overall decrease in the magnitude of α since both types of carrier contribute with an opposite sign.

The dispersion curves of $In_xCo_4Sb_{12}$ for x = 0.0, 0.04, 0.11 and 0.26 show a remarkable evolution of the conduction bands with increasing x (Figures 7a to 7d). It should be stressed here that the calculated energy gap strongly depends on the approach used as well as on the atomic coordinate of Sb, which result in band gap varying from 0.05eV up to 0.3eV in prior studies [2]. This fact was partly attributed to the LDA deficiency and to relativistic effects. The vanishing direct gap at the Γ point (Figure 7a) is rather related here to limitations of LDA and muffin-tin form of the crystal potential employed in the KKR-CPA calculations. This is corroborated by the fact that in Co_4Sb_{12}, our full-potential KKR calculations yielded values of 0.22 eV and 0.09 eV in semi-relativistic and relativistic results, respectively. The reason for these different values of the energy gap and its dependence on the method used in $CoSb_3$ was reported in prior studies [38,39]. Keeping in mind the underestimation of the gap at the Γ point, the variations of the heavy bands at the H point with respect to the light bands near Γ can be analyzed for different In contents. At low In contents (x = 0.04), the Fermi level slightly increases and touches the triply degenerated bands as the number of electrons increases in the system. At higher x values, these heavy bands rapidly shift down (Figures 7c and 7d) and consecutive electrons mainly fill the Fermi surface pockets near the H point, while the filling of the pockets near Γ remains almost constant when increasing x. This behavior suggests that increasing the In concentration in $In_xCo_4Sb_{12}$ should result in modifications in the effective mass of the carriers. For all x values, the conduction bands host the Fermi level indicating an intrinsic n-type electrical conduction. Even though In concentration has little influence on the overall band structure curvature, In does impact the relative position of the bands located around the Γ and H points. Because In provides one electron per atom to the structure (one 5p electron transferred to the conduction band), an increase in x shifts the Fermi level deeper inside the conduction bands and thus, is expected to lead to an increase in the carrier concentration.

3.3 Magnetic susceptibility

For x = 0.0 and 0.04, the isothermal magnetization data $M\left(\mu_0 H\right)$ up to 5T (not shown) remain negative in the entire temperature range indicative of diamagnetic behavior. At higher In contents however, the $M\left(\mu_0 H\right)$ data indicate that a paramagnetic behavior sets in below ~ 75 K. No traces of ferromagnetic impurities were observed in the low-field data down to the lowest temperature. In all samples, the linear variation that prevails above 60K evolves into a non-linear behavior below this temperature suggesting a paramagnetic component presumably due to minute amounts of paramagnetic impurities.

The magnetic susceptibility data derived from $\chi = \left.\frac{\partial M(\mu_0 H)}{\partial H}\right|_{H\to 0}$ are compiled in Figure 8 for all samples. The diamagnetic character of the binary $CoSb_3$ compound is preserved upon introducing low levels of In (x = 0.04). Higher In concentrations lead to positive values of χ below ~ 75 K from x = 0.11 up to x = 0.26. In this paramagnetic regime, a Curie-type tail is discernable and reflects traces of paramagnetic impurities seen in the $M(\mu_0 H)$ data. As x further increases, the χ values decrease in absolute values to tend to a paramagnetic behavior.

To go further, we subtracted the Pauli susceptibility, which arises due to a non-zero $N(E_F)$ to the $\chi(T)$ data. This term was estimated from the experimental $N(E_F)$ values derived from the Sommerfeld coefficient γ using the relation $\gamma = 0.176N(E_F)$ (when γ and $N(E_F)$ are expressed in $mJ.mol^{-1}.K^{-2}$ and $states.Ry^{-1}.(formula\ unit)^{-1}$, respectively). The remaining signal was found to be diamagnetic in the whole x-range implying a diamagnetic state of the In atoms *i.e.* In^{+} or In^{3+}. Comparing these results to our first-principles calculations leads to the conclusion that In is close to a +1 oxidation state in $CoSb_3$.

3.4 Electrical properties

Figure 9 shows the temperature dependence of α for all the samples studied. The main consequence of inserting In is to switch the intrinsic *p*-type electrical conduction of $CoSb_3$ to *n*-type as widely observed in partially-filled skutterudites. [2,3] In absolute values, α slowly decreases from -180 $\mu V.K^{-1}$ (x = 0.04) with increasing x to -150 $\mu V.K^{-1}$ at 300 K for x = 0.26. It is noteworthy that the room-temperature absolute α values are significantly lower than those reported by He *et al*. [4] over the entire In concentration range. Since our values were further corroborated by measurements at high temperatures, it is likely that the values measured in this prior study were slightly overestimated. Both the temperature dependence and the measured values reflect the highly-doped semiconducting nature of the In-filled compounds.

The lower $|\alpha|$ values observed in the partially-filled samples originate from an increase in the electron concentration with respect to $CoSb_3$ as corroborated by the electrical resistivity data shown in Figure 10. The semiconducting behavior of the parent $CoSb_3$ compound turns into a metallic-like regime when In is introduced. As shown in Table 3, the room-temperature variations in the ρ values coincide with that of α.

A deeper understanding of the impact of In on the carrier concentration is given by a comparison of the temperature dependence of the Hall constant R_H shown in Figure 11a. For all In concentrations, the values of R_H are negative indicating the existence of a dominant electronlike signal. In addition, R_H remains practically T-independent, further confirming that these samples behave as heavily-doped semiconductors. These values correspond to a Hall electron density n_H varying by one order of magnitude at 300 K from 2.3×10^{19} for x = 0.04 up to 2.3×10^{20} cm^{-3} for x = 0.26 within a single-band model (see Table 3). However, this analysis relies on the assumption that the Hall factor r_H is equal to 1, which is only valid in degenerate systems or for energy-independent carrier relaxation time. Here, due to the low degree of degeneracy of the samples, this factor can substantially deviate from unity leading to a distinction between the chemical carrier concentration n and the Hall carrier concentration n_H

related by $n = r_H n_H$. For instance, in non-degenerate semiconductors, r_H can vary from 1.18 for scattering by acoustic phonons up to 1.93 for scattering by ionized impurities.

First-principles calculations have shown that the Fermi level intersect bands of similar curvature. Even though the degeneracy of the bands near the H points should be in principle taken into account, we restrict our analyses to a single-parabolic-band model. In this description, r_H is given by [40]

$$r_H = \frac{3}{2} F_{1/2}(\eta) \left[\frac{(1/2 + 2\lambda) F_{2\lambda-1/2}(\eta)}{(1+\lambda)^2 F_\lambda^2(\eta)} \right] \quad (7)$$

where λ is a parameter reflecting the dominant scattering mechanism of electrons, η is the reduced Fermi level and $F_i(\eta)$ is the Fermi integral of *i*th order defined by

$$F_i(\eta) = \int_0^\infty \frac{\xi^i d\xi}{1 + e^{(\xi-\eta)}} \quad (8)$$

where ξ is the reduced carrier energy. Using the values of η derived from the analysis of the thermopower data (see below), r_H can be calculated with $\lambda = 0$ for acoustic phonon scattering (see Table 4). The values obtained remain very similar (r_H ~ 1.12) in the electron concentration range investigated.

The Hall mobility $\mu_H = R_H / \rho$ shows a T-dependence similar to those observed for various filler elements (Figure 11b). Two mechanisms of electron scattering are readily discernable. Below 50 K, the constant μ_H values indicate neutral-impurity scattering while above this temperature, a clear trend towards acoustic-phonon scattering appears ($\mu_H \propto T^{-3/2}$). The values of μ_H range between 37 and 106 $cm^2.V^{-1}.s^{-1}$ at 300 K in the x = 0.26 and 0.04 samples, respectively, and increase up to ~ 2500 $cm^2.V^{-1}.s^{-1}$ below 50 K. These values compare well with those observed in single crystalline $CoSb_3$ or in other partially-filled skutterudites [2,3].

Combining the α and n data, the effective mass of the electrons m^* may be estimated within the above-mentioned assumption of a single-parabolic-band model for which, α and n are expressed as [40]

$$\alpha = \frac{k_B}{e}\left[\frac{(2+\lambda)F_{1+\lambda}(\eta)}{(1+\lambda)F_{\lambda}(\eta)} - \eta\right] \tag{9}$$

$$n_H = 4\pi\left(\frac{2m^* k_B T}{h^2}\right)^{3/2} \frac{F_{1/2}(\eta)}{r_H} \tag{10}$$

At 300 K, this model leads to effective masses ranging between 1.1 and $3.4\,m_0$ (m_0 is the bare electron mass) using the experimental α and n values. The overall increase in m^* with *x* support the accuracy of our band-structure calculations predicting changes in the effective mass due to the shift of the bands at the H points of the Brillouin zone.

One of the most relevant information regarding fine-tuning of the carrier concentration is related to the actual number of electrons provided per In atoms. Within a pure ionic picture and based on the magnetic susceptibility data and band structure calculations, one would expect one electron per atom to be transferred to the host framework *i.e.* an oxidation state of +1. Yet, as demonstrated with other filling species and except for the particular case of Tl [11], a complete ionization of the guest atoms is never observed at 300 K. The degree of ionization can be estimated by plotting n versus the concentration of In atoms (not shown) yielding in the present case ~ 0.4 electron per In atom. This result further corroborates the idea that In takes the monovalent In^+ state.

3.5 Thermal properties

In addition to providing an interesting experimental window into the lattice dynamics of skutterudites, specific heat measurements help to elucidate the evolution of $N(E_F)$ with *x*. This dependence is captured by the low-temperature $C_p(T)$ data, which can be usually described by the free-

electron formula $C_p/T = \gamma + \beta T^2$ where γ and βT^2 are the electronic and phononic contributions, respectively. This relation is expected to hold at temperatures below $\sim\theta_D/50$ (θ_D is the Debye temperature) *i.e.* in a temperature range where only long-wavelength acoustic phonon modes are excited. In partially-filled skutterudites, the value of θ_D is ~ 300 K, practically independent of the nature of the filler element. The above-mentioned relation is therefore expected to be adequate below ~ 6 K. As shown in Figure 12a, where C_p/T is plotted as a function of T^2 for *x* = 0.0, 0.11 and 0.26, a linear-in-*T* behavior up to 7 K is evidenced indicating the relevance of the Debye model to describe the low-temperature $C_p(T)$ data in these compounds. Fitting $C_p(T)$ between 2 and 7 K to this formula yields the values of the γ and β coefficients, listed in Table 5. The γ values increase with *x*, a trend being well reproduced by our first-principles calculations and indicating a progressive shift of the Fermi level towards the conduction bands upon alloying with In.

The β parameter varies only little with the In content and is linked to the Debye temperature via the formula $\theta_D = \left[\left(12\pi^4 RN\right)/\left(5\beta\right)\right]^{1/3}$ where R is the gas constant and N is the number of atoms per chemical formula ($16 + x$ in the present case). This yields θ_D values ranging between 325 K for $CoSb_3$ to 315 K for *x* = 0.26 in very good agreement with that inferred from sound velocity measurements.

Above 7 K, the description within the Debye model is no longer valid as shown by the $C_p(T)$ data, which clearly deviate from the simple T^3 law. This loss of linearity is the signature indicating that excitations other than long-wavelength acoustic phonons start playing a role. Likewise in cage-like compounds such as clathrates or pyrochlores [41-46], these modes appear as a pronounced hump when plotting C_p/T^3 vs T (Figure 12b), which can be described by an additional Einstein-like contribution existing over a Debye background following the expression

$$C_p(T) = \gamma T + 9N_D\left(\frac{T}{\theta_D}\right)^2 \int_0^{\theta_D/T} \frac{x^4 e^x}{(e^x-1)^2}\,dx + \sum_i p_i N_{Ei} R\left(\frac{\theta_{Ei}}{T}\right)^2 \frac{e^{\theta_{Ei}/T}}{(e^{\theta_{Ei}/T}-1)^2} \qquad (11)$$

where $x = \hbar\omega / k_B T$ with $\hbar = h / 2\pi$ (h is the Planck constant), N_D is the number of Debye oscillators per formula unit and p_i, N_{Ei} and θ_{Ei} are the degrees of freedom, the number of Einstein oscillators, and the Einstein temperature related to the *i*th vibrational mode, respectively. Several crystallographic studies have shown that the thermal motion of the filler element inside the voids can be considered as isotropic so that no distinction between the in-plane and out-of-plane vibrations is required such as, for instance, in clathrates [40-43]. The thermal motion of In can be therefore modeled with only one isotropic Einstein oscillator so that $p_1 N_{E1}$ is fixed to $p_1 N_{E1} = 3 \times x$. The Einstein temperature θ_{E1} is then deduced from least-square fit to the data according to Eq.(11) and results in θ_{E1} = 65 K in good agreement with the inelastic neutron scattering data of Peng *et al*. [26]

To further characterize the thermal properties of these compounds, the Grüneisen parameter γ_G, which represents a measure of the bonding anharmonicity, can be inferred from a combination of the thermodynamic and elastic properties following the formula

$$\gamma_G = \frac{3\beta B V_m}{C_V} \tag{12}$$

where β is the volume thermal expansion coefficient, B is the isothermal bulk modulus, V_m is the molar volume and C_V is the isochoric specific heat. Because of the cubic crystal lattice of skutterudites, the β parameter was taken as three times the linear thermal expansion coefficient *i.e.* β = 27.10^{-6} K^{-1}. B was determined from the transverse and longitudinal sound velocities by

$$B = d\left(v_L^2 - \frac{4}{3}v_T^2\right) \tag{13}$$

and was found to be B ~ 90.2 GPa at 300 K. C_V was estimated assuming that the difference between the isochoric and isobaric specific heats is negligibly small in solids near room temperature. The

experimental C_p value of 0.225 J.g^{-1}.K^{-1} at 300 K was therefore used in the present analysis. Using these values, Eq.(13) yields γ_G = 0.72. This value, slightly lower than those derived for $CoSb_3$ (0.95 and 1.11 in Ref. 47 and 48, respectively), can be compared to those obtained in materials exhibiting high anharmonicity such as in PbTe, $Cu_2Ga_{0.1}Ge_{0.9}Se_3$ or $AgSbTe_2$ for which γ_G = 1.45, 1.70 and 2.05, respectively [49-51] The lower value obtained for these In-filled skutterudites thus suggests that these compounds show only little anharmonicity.

Figure 13a presents the temperature dependence of the total thermal conductivity. The overall evolution of the $\kappa(T)$ data follows the general behavior observed in single- and multiple-filled skutterudites [2,3]. One of the main features is related to the magnitude of the low-temperature peak value that is strongly lowered with increasing *x*. Near room temperature, the different curves practically merge into a single one suggesting a less pronounced influence of the In atoms on κ at high temperatures. To properly disentangle the electronic from the lattice contribution, the Lorenz number $L = \kappa_e \rho / T$ was calculated at 300 K following the formula [40]

$$L = \frac{k_B^2}{e^2} \frac{(1+\lambda)(3+\lambda)F_\lambda(\eta)F_{2+\lambda}(\eta) - (2+\lambda)^2 F_{1+\lambda}(\eta)^2}{(1+\lambda)^2 F_\lambda(\eta)^2} \quad (14)$$

using $\lambda = 0$ and the η values derived from Eq.(9). The values obtained within this model, listed in Table 4, are significantly lower than the value of a degenerate electron gas *i.e.* L_0 = 2.45×10^{-8} V^2.K^{-2}. The presence of In in the voids leads to an overall lower lattice thermal conductivity with respect to $CoSb_3$ (Figure 13b). The minimum value of 3.3 W.m^{-1}.K^{-1} at 300 K was measured for the *x* = 0.26 sample (see Table 2). Given the rather low Grüneisen parameter, this significant decrease is likely due to enhanced phonon scattering arising from a combined increase in point-defect scattering and mass fluctuations between the filled and empty voids.

3.6 High-temperature thermoelectric properties

The high-temperature thermoelectric properties are shown in Figures 14a to 14d. The ρ data rises with increasing temperature due to increasing electron-phonon scattering events (Figure 14a). While the $\rho(T)$ data of the x = 0.04 sample show a maximum and then decreases, higher In contents result in metallic-like behavior in the whole temperature range. The observed maximum likely marks the onset of thermal activation of minority carriers as suggested by the minimum visible both in the thermopower and thermal conductivity data.

As already seen in the low-T data, all the samples show large thermopower values that slightly increase (in absolute values) up to a maximum temperature before decreasing at higher temperatures (Figure 14b). The minimum observed correlates with those observed in $\kappa(T)$ indicating the contribution of minority carriers to transport. This behavior offers an alternative way to estimate the thermal band gap from the maximum α value (in absolute values) occurring at the temperature $T_{\max}$ via $E_g = 2e\alpha_{\max}T_{\max}$. Note that in the present case, this gap corresponds to an indirect gap that exists between the top of the conduction bands located in the H-N direction and at the Γ point (see Figure 7). This formula yields an energy gap of ~ 0.3 eV for x = 0.04. As x increases, the maximum is shifted towards higher temperature to be located at 700 K for x = 0.11 and then to be no longer visible in the temperature range covered for x = 0.18 and 0.26. In the former, the higher value of $T_{\max}$ combined with a lower $\alpha_{\max}$ leads to a similar estimation of ~ 0.3 eV indicating only minor changes in the indirect gap with x. This result lends further support to the validity of the rigid-band approximation in the present case.

The high-temperature $\kappa(T)$ data (Figure 14c) show a decrease with temperature as expected in crystalline materials up to the temperature where the bipolar contribution starts playing a role. Below these temperatures, a T^{-1} law should prevail provided phonon-phonon scattering dominates. If this law is approximately followed at low In contents, the observed decay is less strong at higher x values possibly due to a more pronounced influence of point-defect scattering.

The dimensionless thermoelectric figure of merit ZT rises with increasing temperature until the samples enter the intrinsic regime (Figure 14d). Likewise in other partially-filled skutterudite system,

the *ZT* increases with the In content to reach a maximum value of ~ 1.0 at 700 K in the $x = 0.26$ sample. Because of lower α values measured in the present study, this value is significantly lower than those reported by He *et al*. [4] (1.2 at 575 K for $x = 0.22$) and by Mallik *et al*. (1.12 at 650 K for $x = 0.25$) [28].

4. Summary and conclusion

A series of polycrystalline In partially-filled skutterudites $In_xCo_4Sb_{12}$ was synthesized and the evolution of the crystal structure, the thermoelectric and elastic properties as a function of x was investigated. EPMA together with XRPD results indicate a solubility limit of In of $x = 0.26$. Temperature-dependent NPD experiments were used to probe the thermal motion of the In atoms and showed that In can be described by a characteristic Einstein temperature of ~ 67 K in agreement with the low-temperature $C_p(T)$ data. First-principles calculations revealed a DOS near the Fermi level dominated by In *p*-states and a gradual shift of the Fermi level deeper inside the conduction band with increasing x. The highly-doped semiconducting state suggested by these calculations was experimentally confirmed by the $\alpha(T)$ and $\rho(T)$ data between 2 and 800 K. The presence of In has only a weak influence on the elastic properties of $CoSb_3$ and gives rise to a low Grüneisen parameter suggesting a weak bonding anharmonicity in these compounds. The much lower lattice thermal conductivity observed in the In-filled samples in comparison to $CoSb_3$ is thus likely due to a combination of enhanced mass fluctuations and point-defect scattering. At high temperatures, the heavily-doped semiconducting nature of these compounds leads to a maximum *ZT* value of 1.0 at 700 K. Future work on this system should tell us whether In can behave both as a donor and an acceptor dopant in $CoSb_3$.

Acknowledgments

The authors acknowledge support from the European Network of Excellence CMA 'Complex Metallic Alloys' and the project Barrande (7AMB12FR019 –CZ, 26560WD-FR). J. L. acknowledges the

European Space Agency for financial support (ESA/ESTEC Contract C20179). J. T. and K. K. acknowledge support from the National Science Center in Poland (No. DEC-2011/02/A/ST3/00124). Neutron diffraction beamtime at ISIS was provided by the Science and Technology Facilities Council (STFC).

References

[1] *Thermoelectrics Handbook, Macro to Nano,* edited by Rowe D M (CRC Press, Taylor & Francis Group, Boca Raton FL, 2006).

[2] Uher C, in *Semiconductors and Semimetals,* edited by Tritt T (Academic, San Diego, 2000), Vol. 69, p. 139.

[3] Uher C, in *Thermoelectrics and its Energy Harvesting,* edited by Rowe D M(CRC Press, 2012), Chap. 10.

[4] He T, Chen J, Rosenfeld H D and Subramanian M A 2006 *Chem. Mat.* **18** 759

[5] Chen L D, Kawahara T, Tang X F, Goto T, Hirai T, Dyck J S, Chen W and Uher C 2001 *J. Appl. Phys.* **90** 1864

[6] Nolas G S, Kaeser M, Littleton IV R T and Tritt T M 2000 *Appl. Phys. Lett.* **77** 1855

[7] Puyet M, Lenoir B, Dauscher A, Pécheur P, Bellouard C, Tobola J and Hejtmanek J 2006 *Phys. Rev. B* **73** 035126

[8] Pei Y Z, Chen L D, Zhang W, Shi X, Bai S Q, Zhao X Y, Mei Z G and Li X Y 2006 *Appl. Phys. Lett.* **89** 221107

[9] Pei Y Z, Bai S Q, Zhao X Y, Zhang W and Chen L D 2008 *Solid State Sci.* **10** 1422

[10] Zhang J, Xu B, Wang L M, Yu D, Liu Z, He J and Tian Y 2011 *Appl. Phys. Lett.* **98** 072109

[11] Sales B C, Chakoumakos B C and Mandrus D 2000 *Phys. Rev. B* **61** 2475

[12] Morelli D T, Meisner G P, Chen B, Hu S and Uher C 1997 *Phys. Rev. B* **56** 7376

[13] Pei Y Z, Yang J, Chen L D, Zhang W, Salvador J R and Yang J 2009 *Appl. Phys. Lett*. **95** 042101

[14] Zhao X Y, Shi X, Chen L D, Zhang W Q, Zhang W B and Pei Y Z 2006 *J. Appl. Phys.* **99** 053711

[15] Bai S Q, Shi X and Chen L D 2010 *Appl. Phys. Lett.* **96** 202102

[16] Shi X, Kong H, Li C P, Uher C, Yang J, Salvador J R, Wang H, Chen L and Zhang W 2008 *Appl.*

Phys. Lett. **92** 182101

[17] Zhao W Y, Dong C L, Wie P, Guan W, Liu L S, Zhai P C, Tang X F and Zhang Q J 2007 *J. Appl. Phys.* **102** 113708

[18] Su X, Li H, Yan Y, Chi H, Tang X, Zhang Q and Uher C 2012 *J. Mat. Chem*. **22** 15628

[19] Peng J Y, Alboni P N, He J, Zhang B, Su Z, Holgat T, Gothard N and Tritt T M 2008 *J. Appl. Phys.* **104** 053710

[20] Zhao W, Wei P, Zhang Q, Dong C, Liu L and Tang X 2009 *J. Am. Chem. Soc*. **131** 3713

[21] Harnwunggmoung A, Kurosaki K, Kosuga A, Ishimaru M, Plirdpring T, Yimnirun R, Jutimoosik J, Rujirawat S, Ohishi Y, Muta H and Yamanaka S 2012 *J. Appl. Phys.* **112** 043509

[22] Shi X, Yang J, Salvador J R, Chi M, Cho J Y, Wang H, Bai S, Yang J, Zhang W and Chen L 2012 *J. Am. Chem. Soc.* **134** 2842

[23] Li H, Tang X, Zhang Q and Uher C 2009 *Appl. Phys. Lett.* **94** 102114

[24] Tang G D, Wang Z H, Xu X N, He Y, Qiu L and Du Y W 2011 *J. Elec. Mater.* **40** 611

[25] Tang G, Zhang D, Chen G, Xu F and Wang Z 2013 *Physica B* **408** 79

[26] Peng J, Xu W, Yan Y, Yang J, Fu L, Kang H and He J 2012 *J. Appl. Phys.* **112** 024909

[27] Eilertsen J, Rouminov S and Subramanian M A 2012 *Acta Mater.* **60** 2178

[28] Mallik R C, Jung J Y, Ur S C and Kim I H, 2008 *Met. Mater. Int.* **14** 223

[29] Mallik R C, Stiewe C, Karpinski G, Hassdorf R and Müller E, 2009 *J. Elec. Mater.* **38** 1337

[30] Qiu Y, Xi L, Shi X, Qiu P, Zhang W, Chen L, Salvador J R, Cho J Y, Yang J, Chien Y C, Chen S, Tang Y and Snyder G J 2013 *Adv. Funct. Mater.* DOI: 10.1002/adfm.201202571

[31] Puyet M, Lenoir B, Dauscher A, Candolfi C, Hejtmanek J, Stiewe C and Müller E 2012 *Appl. Phys. Lett.* **101** 222105

[32] Rodriguez-Carvajal J 1993 *Physica B* **192** 55-69

[33] Korringa J 1947 *Physica* **13** 392; Kohn W and Rostoker N 1954 *Phys. Rev.* **94** 1111

[34] Bansil A, Kaprzyk S, Mijnarends P E and Tobola J 1999 Phys. Rev. B **60** 13396

[35] Rogl G, Zhang L, Rogl P, Grytsiv A, Falmbigl M, Rajs D, Kriegisch M, Müller H, Bauer E, Koppensteiner J, Schranz W, Zehetbauer M, Henkie Z and Mapple M B 2010 *J. Appl. Phys.* **107** 043507

[36] Mi J L, Christensen M, Nishibori E and Iversen B B 2011 *Phys. Rev. B* **84** 064114

[37] Anderson O L 1963 *J. Phys. Chem. Solids* **24** 909

[38] Singh D J, Pickett W E 1994 *Phys. Rev. B* **50** 11235

[39] Sofo J O, Mahan G D 1998 *Phys. Rev. B* **58** 15620

[40] Fistul V I, *Heavily Doped Semiconductors* (Plenum Press, New York, 1969)

[41] K. Matsuhira, C. Sekine, M. Wakeshima, Y. Hinatsu, T. Namiki, K. Takeda, I. Shirotani, H. Sugawara, D. Kikuchi and H. Sato, J. Phys. Soc. Japan **78**, 124601 (2009).

[42] Aydemir U, Candolfi C, Ormeci A, Oztan Y, Baitinger M, Oeschler N, Steglich F and Grin Y 2011 *Phys. Rev. B* **84** 195137

[43] Aydemir U, Candolfi C, Borrmann H, Baitinger M, Ormeci A, Carrillo-Cabrera W, Chubilleau C, Lenoir B, Dauscher A, Oeschler N, Steglich F and Grin Y 2010 *Dalton Trans.* **39** 1078

[44] Suekuni K, Avila M A, Umeo K and Takabatake T 2007 *Phys. Rev. B* **75** 195210

[45] Avila M A, Suekuni K, Umeo K, Fukuoka H, Yamanaka S and Takabatake T 2006 *Phys. Rev. B* **74** 125109

[46] Melot B C, Tackett R, O'Brien J, Hector A L, Lawes G, Seshadri R and Ramirez A P 2009 *Phys. Rev. B* **79** 224111

[47] Slack G A and Tsoukala V G 1994 *J. Appl. Phys.* **76** 1665

[48] Chi H, Kim H, Thomas J C, Su X, Stackhouse S, Kaviany M, Van der Ven A, Tang X and Uher C 2012 *Phys. Rev. B* **86** 195209

[49] Slack G A, in *Solid State Physics,* edited by Ehrenreich H, Weitz F and Turnbull D (Academic Press, New York, 1979), Vol. 34, pp. 1–71.

[50] Cho J Y, Shi X, Salvador J R, Meisner G P, Yang J, Wang H, Wereszczak A A, Zhou X and Uher C 2011 *Phys. Rev. B* **84** 085207

[51] *Physics of Non-tetrahedrally Bonded Binary Compounds II,* Landolt-Börnstein Numerical Data and Functional Relationships in Science and Technology, Group III, Vol. 17, edited by Subvol. F (Springer, Berlin, 1983), p. 419, Fig. 18.

Tables

Table 1. Nominal, actual compositions measured by EPMA and lattice parameters (*a*) inferred from XRPD of the $In_xCo_4Sb_{12}$ compounds.

Nominal composition	EPMA	a (Å)
Co_4Sb_{12}	$Co_4Sb_{12.24}$	9.0360
$In_{0.1}Co_4Sb_{12}$	$In_{0.04}Co_4Sb_{12}$	9.0407
$In_{0.2}Co_4Sb_{12}$	$In_{0.11}Co_4Sb_{12}$	9.0442
$In_{0.30}Co_4Sb_{12}$	$In_{0.18}Co_4Sb_{12}$	9.0504
$In_{0.4}Co_4Sb_{12}$	$In_{0.26}Co_4Sb_{12}$	9.0523

Table 2. Atomic positions and isotropic displacement parameters of the illustrative $x = 0.26$ sample. The occupancy of the In site was kept constant to the value measured by EPMA.

Atom	Site	*x*	*y*	*z*	U_{iso} (Å^2)	occupancy (%)
			300 K			
In	2a	0	0	0	0.022(8)	26
Co	8c	0.25	0.25	0.25	0.004(7)	100
Sb	24g	0	0.335(3)	0.157(8)	0.005(7)	100
			220 K			
In	2a	0	0	0	0.016(0)	26
Co	8c	0.25	0.25	0.25	0.003(1)	100
Sb	24g	0	0.335(2)	0.157(6)	0.003(9)	100
			150 K			
In	2a	0	0	0	0.012(5)	26
Co	8c	0.25	0.25	0.25	0.002(5)	100
Sb	24g	0	0.335(4)	0.157(6)	0.002(6)	100
			80 K			
In	2a	0	0	0	0.008(4)	26
Co	8c	0.25	0.25	0.25	0.001(7)	100
Sb	24g	0	0.335(9)	0.157(6)	0.001(6)	100
			4 K			
In	2a	0	0	0	0.002(4)	26
Co	8c	0.25	0.25	0.25	0.001(7)	100
Sb	24g	0	0.335(4)	0.157(6)	0.001(1)	100

Table 3. Room temperature values of the electron concentration (n), thermopower (α), electrical resistivity (ρ), total thermal conductivity (κ) and lattice (κ_L) and electronic (κ_e) thermal conductivities of $In_xCo_4Sb_{12}$.

x	n (10^{19} cm^{-3})	α ($\mu V.K^{-1}$)	ρ ($\mu\Omega.m$)	κ ($W.m^{-1}.K^{-1}$)	κ_e ($W.m^{-1}.K^{-1}$)	κ_L ($W.m^{-1}.K^{-1}$)
0.04	2.6	-175	24.0	5.50	0.20	5.30
0.11	8.5	-163	11.0	4.00	0.45	3.55
0.18	10.6	-157	7.4	4.30	0.70	3.60
0.26	25.7	-148	6.5	4.10	0.80	3.30

Table 4. Effective mass (m^*/m_0), reduced Fermi level (η) and Lorenz number (L) estimated at 300 K using equations (7), (9), (10) and (14).

x	r_H	m^*/m_0	η	L ($\times 10^{-8}$ $V^2.K^{-2}$)
0.04	1.13	1.1	0.16	1.63
0.11	1.12	2.3	0.28	1.64
0.18	1.11	2.1	0.80	1.70
0.26	1.10	3.4	1.0	1.72

Table 5. Values of the γ and β parameters inferred from low temperature specific heat analyses. The Debye temperatures θ_D derived from the β parameters are also given.

x	γ ($mJ.mol^{-1}.K^{-2}$)	β ($mJ.mol^{-1}.K^{-4}$)	θ_D (K)
0.0	0.0	0.89	327
0.18	16.2	1.12	314
0.26	18.0	0.96	320

Figure Caption

Figure 1: Rietveld refinement of the time-of-flight neutron diffraction pattern of the x = 0.26 sample at 300 K. The non-fitted data near 2.1 Å correspond to extrinsic reflections coming from the vanadium can and the cryostat used for these experiments.

Figure 2: Temperature dependence of the lattice parameter a of the x = 0.26 sample derived from Rietveld refinements of the NPD data.

Figure 3: Total DOS of $In_xCo_4Sb_{12}$ for x = 0.04, 0.11 and 0.26. The Fermi level is positioned at zero energy.

Figure 4: Site-decomposed DOS of the x = 0.04 (left panel) and x = 0.26 (right panel) compounds. For In atoms, *s*- and *p*-DOS contributions are shown. The Fermi level is positioned at zero energy.

Figure 5: Site-decomposed DOS of $Ca_{0.18}Co_4Sb_{12}$. For Ca, *s*-, *p*- and *d*-DOS contributions are also shown. The Fermi level is positioned at zero.

Figure 6: Site-decomposed DOS of the hypothetical $Co_4Sb_{11.96}In_{0.04}$ compound.

Figure 7: Complex energy band structure of $In_xCo_4Sb_{12}$ for x = 0.04 (a) and 0.11 (b) plotted along high-symmetry directions in the *bcc* Brillouin zone. The Fermi level is represented by the horizontal dashed line at zero.

Figure 8: Magnetic susceptibility as a function of temperature for x = 0.0 (○), 0.04 (□), 0.11 (△), 0.18 (∇) and 0.26 (◊).

Figure 9: Temperature dependence of the thermopower of the x = 0.0 (○), 0.04 (□), 0.11 (Δ), 0.18 (∇) and 0.26 (◊) samples.

Figure 10: Temperature dependence of $\log \rho$ of the x = 0.0 (○), 0.04 (□), 0.11 (Δ), 0.18 (∇) and 0.26 (◊) samples.

Figure 11: Temperature dependence of the Hall coefficient R_H (a) and of the Hall mobility μ_H (b) of the x = 0.0 (○), 0.04 (□), 0.11 (Δ), 0.18 (∇) and 0.26 (◊) samples. Below ~ 30 K, μ_H is constant indicative of scattering by neutral impurities. At higher temperatures, $\mu_H(T)$ follows a $T^{-3/2}$ law characteristic of acoustic-phonon scattering.

Figure 12: (a) C_p/T versus T^2 of the x = 0.0 (○), 0.11 (Δ) and 0.26 (◊) samples highlighting the linear-in-T variation (solid black line) as expected from a conventional Fermi-liquid behavior. (b) Specific heat data plotted as C_p/T^3 vs T to visualize the additional contribution that can be modeled by an Einstein-like term.

Figure 13: (a) Total and (b) lattice thermal conductivity as a function of temperature for x = 0.0 (○), 0.04 (□), 0.11 (Δ), 0.18 (∇) and 0.26 (◊). The lattice contribution was estimated using degeneracy-adjusted Lorenz numbers using a single-parabolic-band model.

Figure 14: High-temperature dependence of the electrical resistivity (a), thermopower (b), thermal conductivity (c) and ZT (d) of the x = 0.0 (○), 0.04 (□), 0.11 (Δ), 0.18 (∇) and 0.26 (◊) samples.

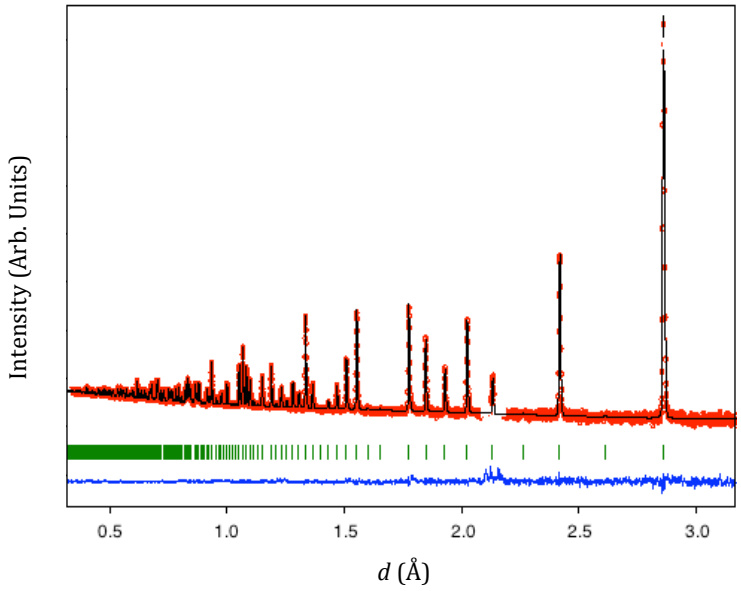

Figure 1

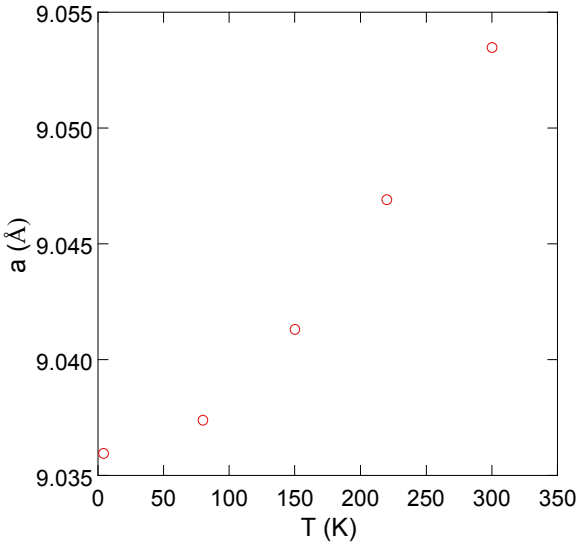

Figure 2

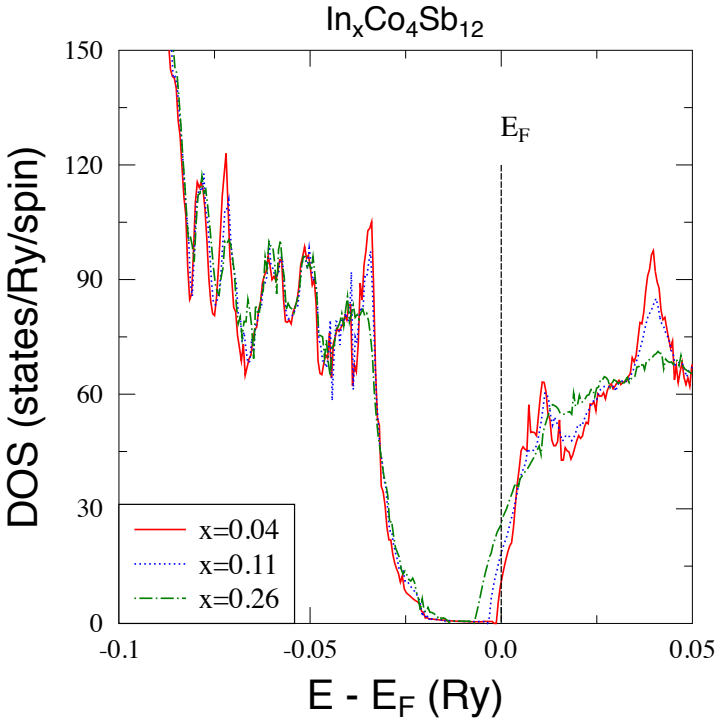
In$_x$Co$_4$Sb$_{12}$
DOS (states/Ry/spin)
E - E$_F$ (Ry)
E$_F$
x=0.04
x=0.11
x=0.26
150
120
90
60
30
0
-0.1
-0.05
0.0
0.05

Figure 3

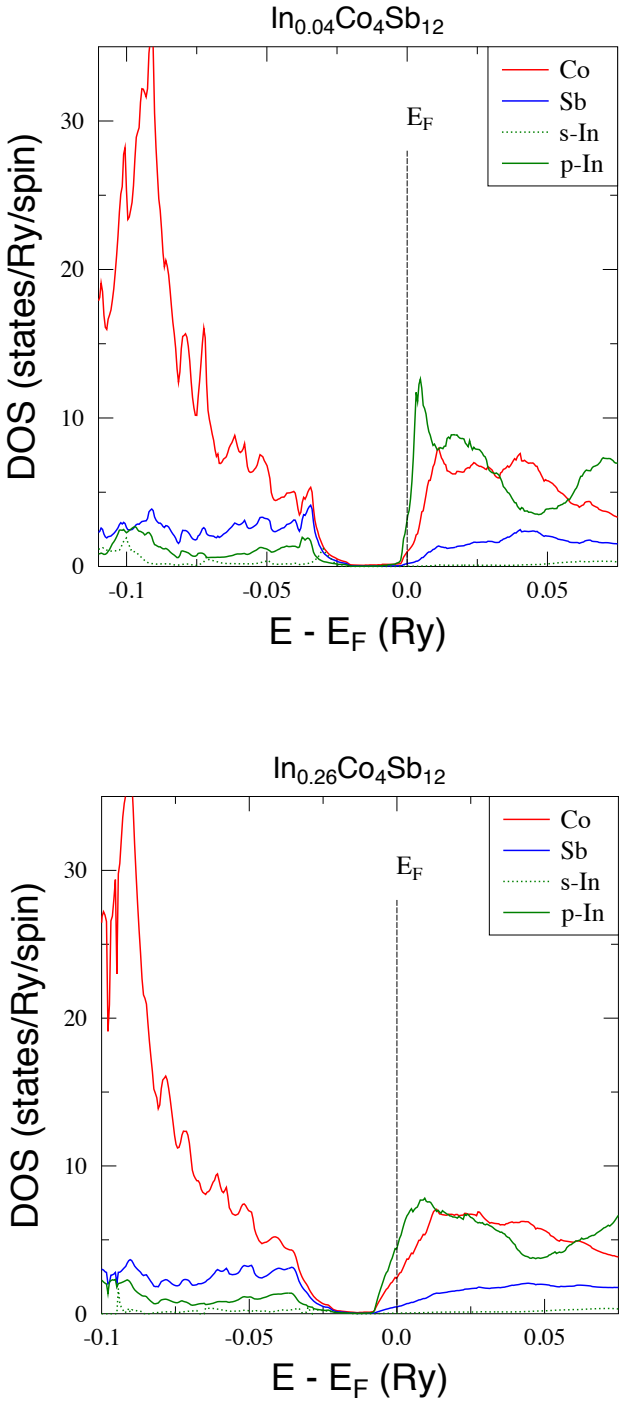
In0.04Co4Sb12
Co
Sb
s-In
p-In
EF
DOS (states/Ry/spin)
E - EF (Ry)
In0.26Co4Sb12
Co
Sb
s-In
p-In
EF
DOS (states/Ry/spin)
E - EF (Ry)

Figure 4

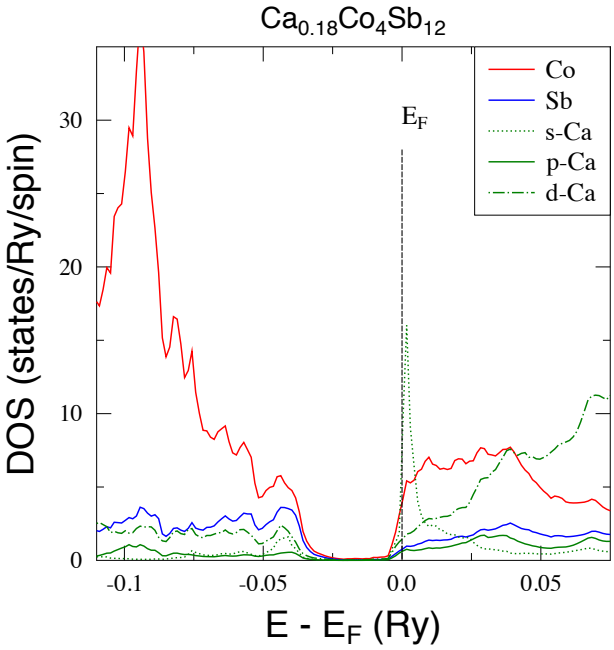
Ca0.18Co4Sb12
Co
Sb
s-Ca
p-Ca
d-Ca
EF
DOS (states/Ry/spin)
30
20
10
0
-0.1
-0.05
0.0
0.05
E - EF (Ry)

Figure 5

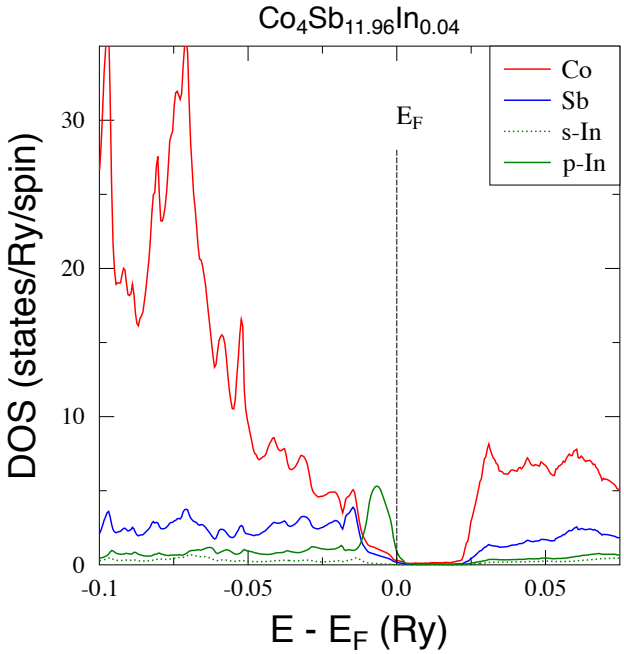
Co4Sb11.96In0.04
Co
Sb
s-In
p-In
EF
DOS (states/Ry/spin)
30
20
10
0
-0.1
-0.05
0.0
0.05
E - EF (Ry)

Figure 6

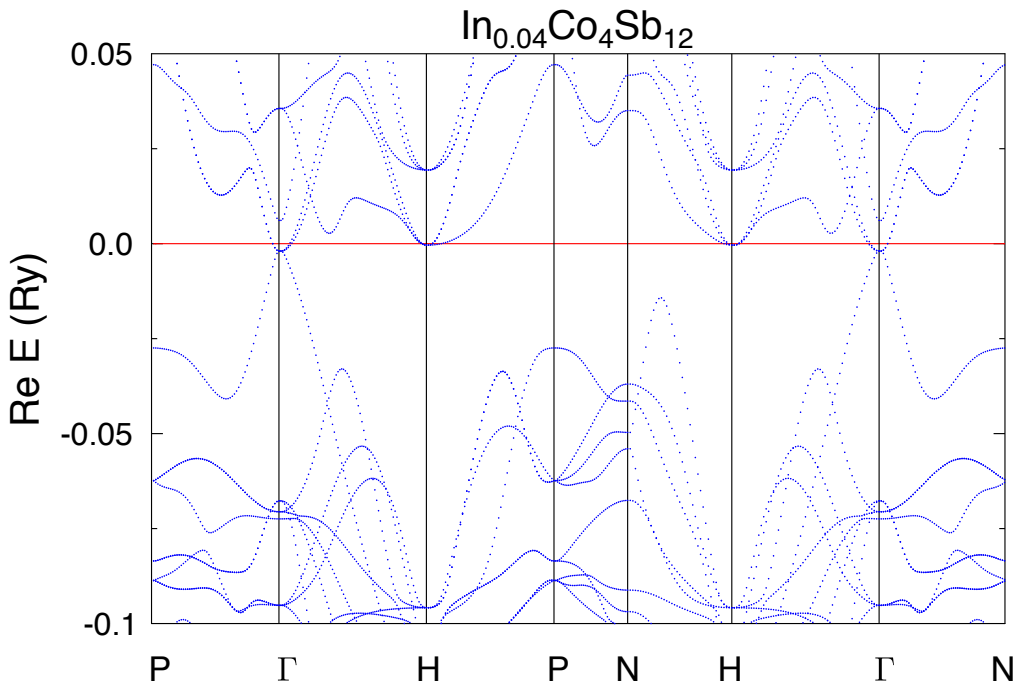
In0.04Co4Sb12
0.05
0.0
-0.05
-0.1
Re E (Ry)
P
Γ
H
P
N
H
Γ
N

(a)

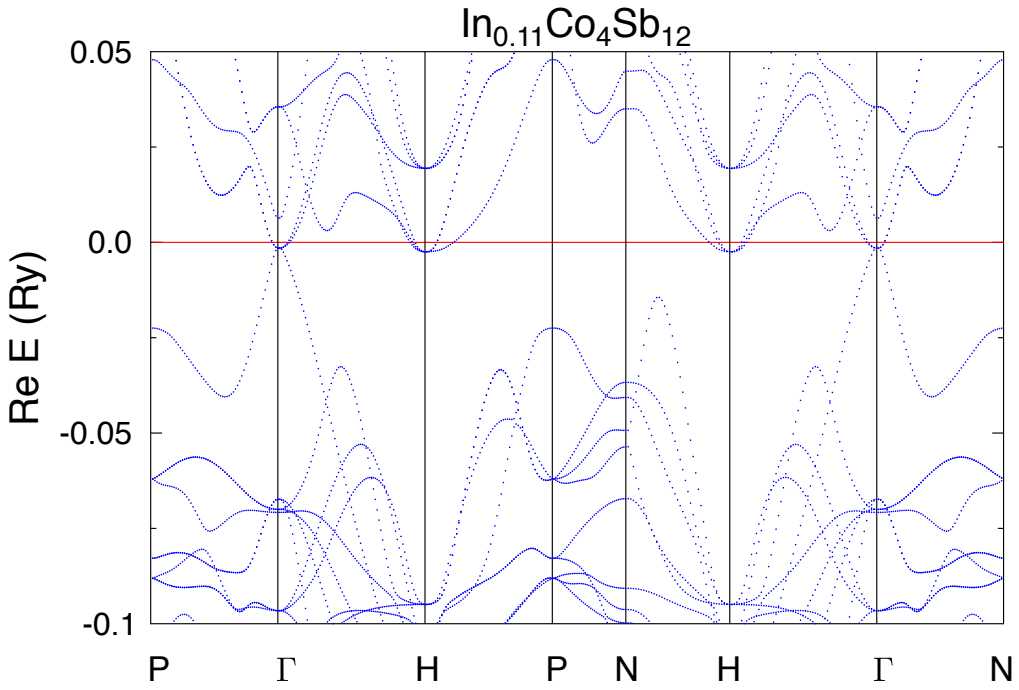
In0.11Co4Sb12
0.05
0.0
-0.05
-0.1
Re E (Ry)
P
Γ
H
P
N
H
Γ
N

(b)

Figure 7

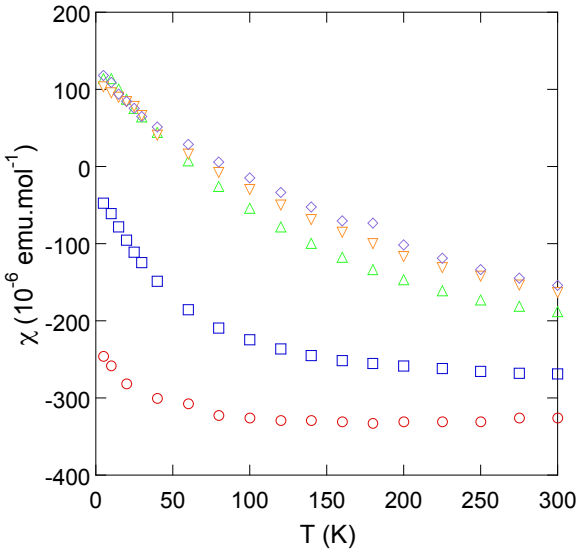
200
100
0
-100
-200
-300
-400
0
50
100
150
200
250
300
T (K)
χ (10-6 emu.mol-1)

Figure 8

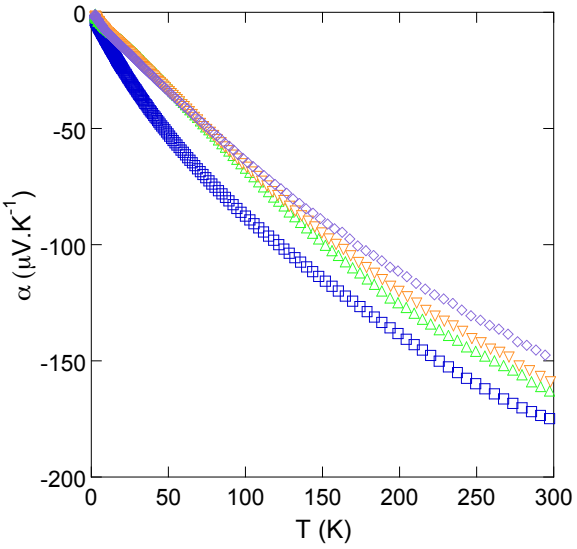

Figure 9

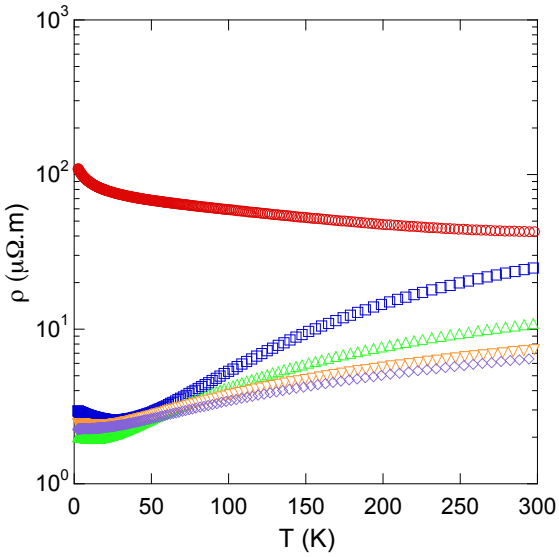

Figure 10

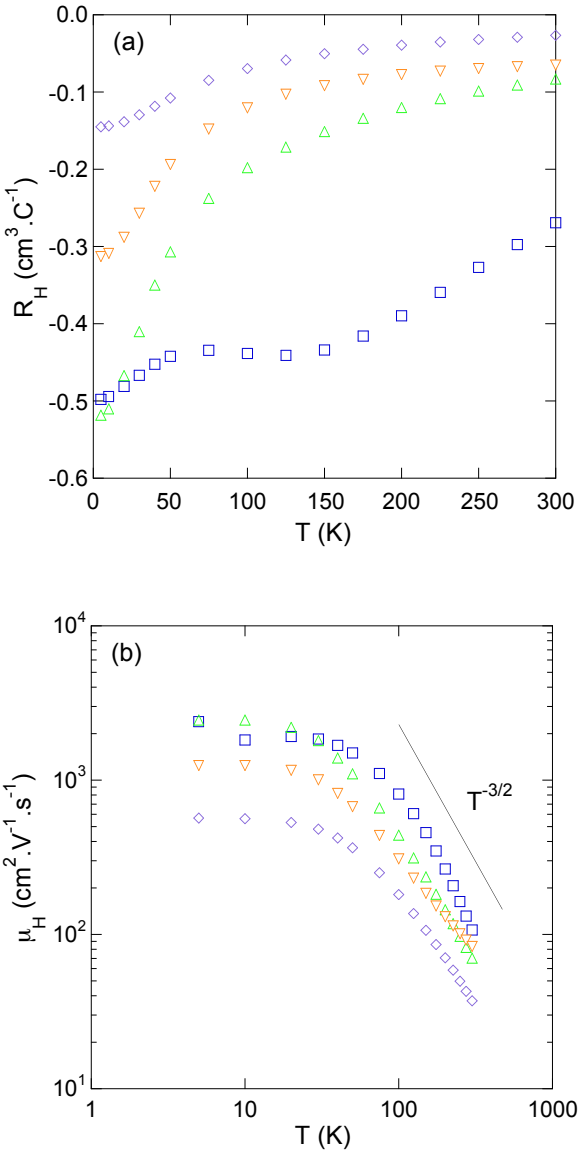
(a)
0.0
-0.1
-0.2
-0.3
-0.4
-0.5
-0.6
R_H ($cm^3.C^{-1}$)
0
50
100
150
200
250
300
T (K)
(b)
10^4
10^3
10^2
10^1
μ_H ($cm^2.V^{-1}.s^{-1}$)
$T^{-3/2}$
1
10
100
1000
T (K)

Figure 11

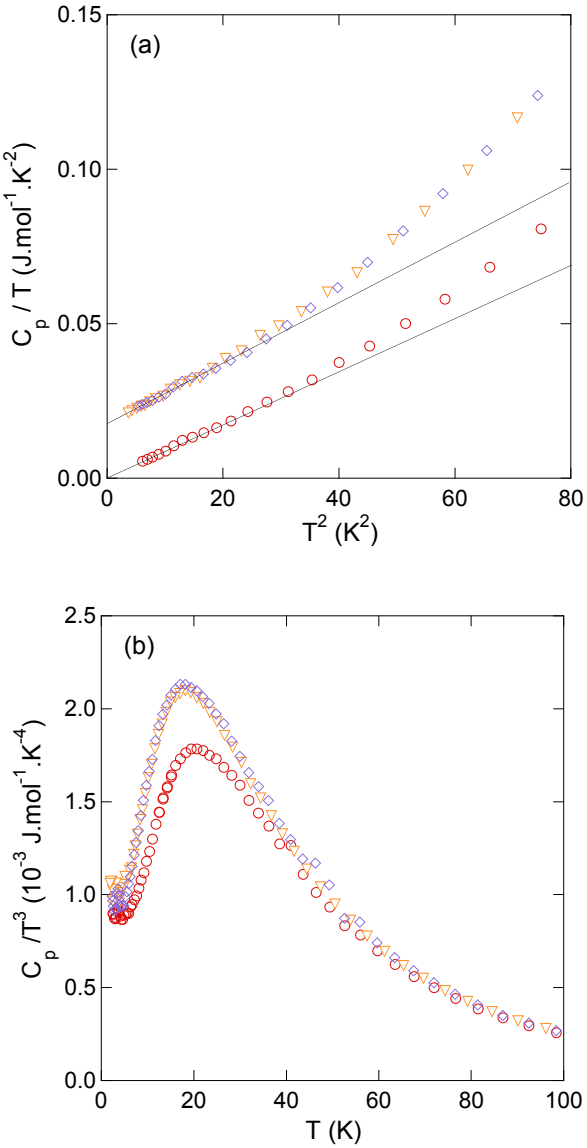
(a)
0.15
0.10
0.05
0.00
0
20
40
60
80
C_p / T (J.mol^{-1}.K^{-2})
T^2 (K^2)
(b)
2.5
2.0
1.5
1.0
0.5
0.0
0
20
40
60
80
100
C_p/T^3 (10^{-3} J.mol^{-1}.K^{-4})
T (K)

Figure 12

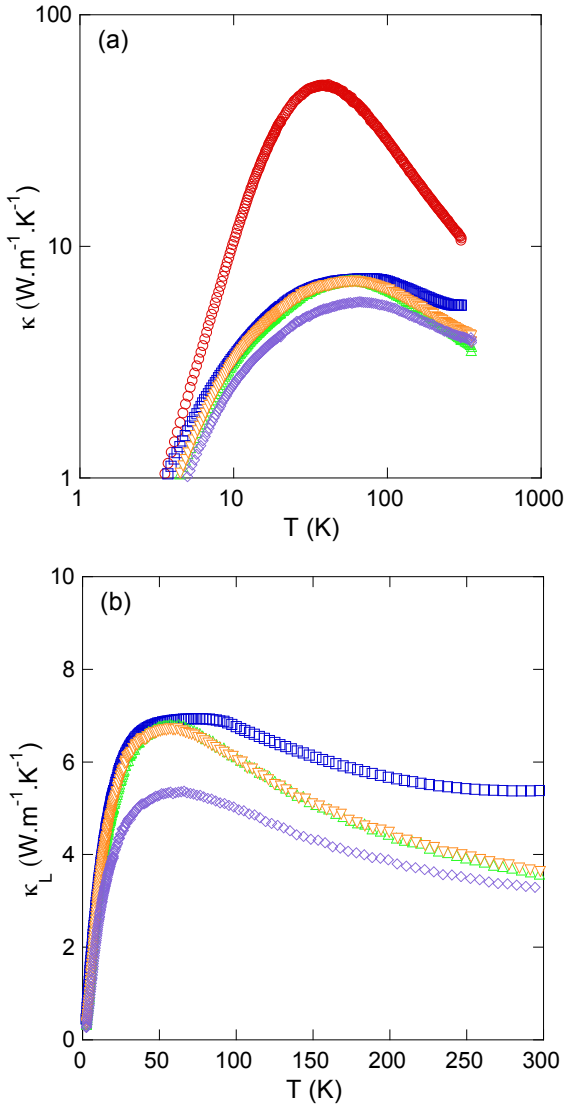

Figure 13

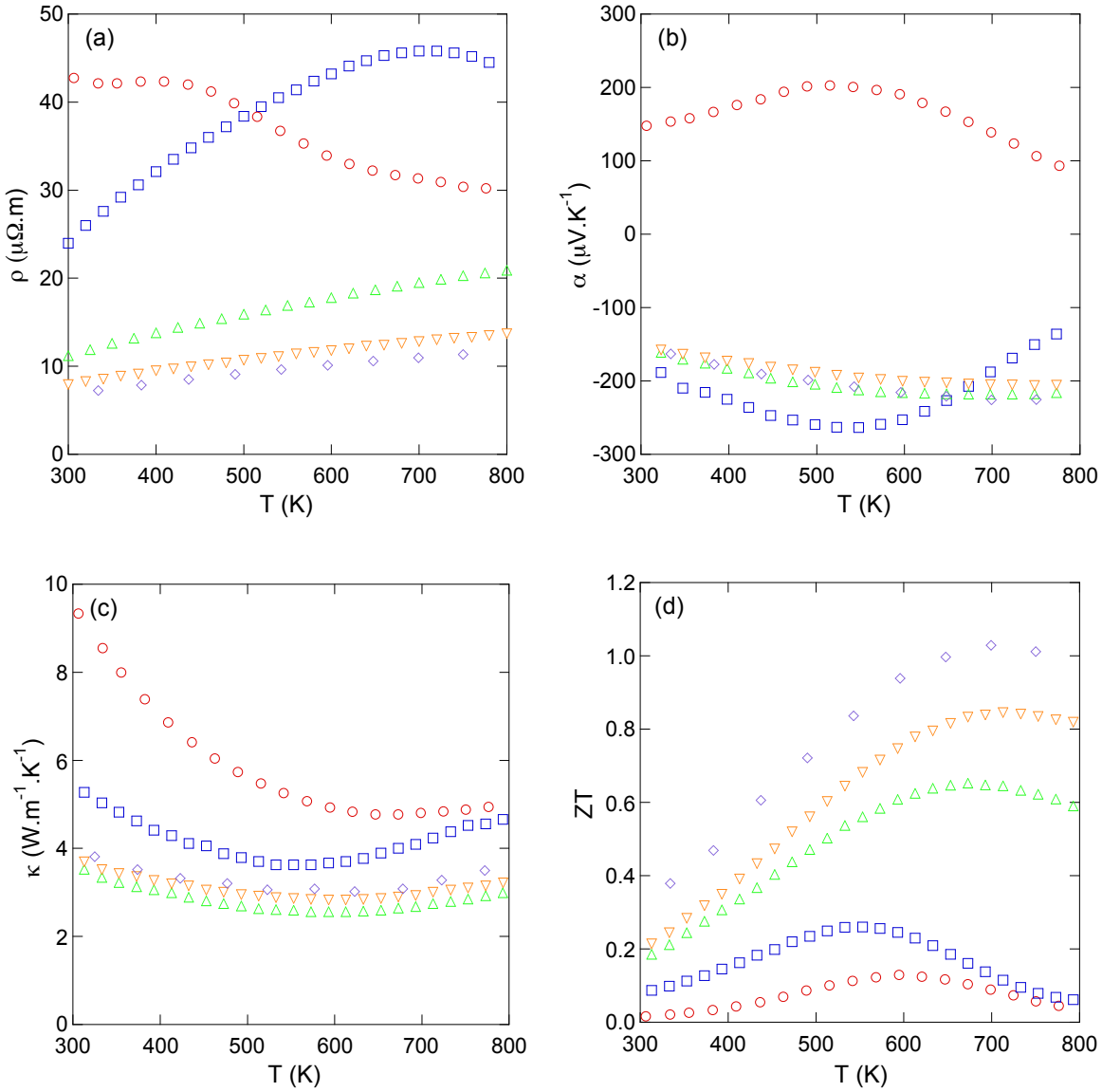

Figure 14